TRENDS IN SCIENCES 2026; 23(3): 11747
https://doi.org/10.48048/tis.2026.11747 RESEARCH ARTICLE

Enhanced Biodiesel production with Cu-doped ZnO Nanocatalyst: A Comprehensive Study on Kinetics, Optimization and Catalytic Performance

Zain Aziz Sayhood* and Ziad Tariq Alismaeel

Department of Biochemical Engineering, Al-Khwarizmi College of Engineering, University of Baghdad, Baghdad Governorate, Iraq

(*Corresponding author's e-mail: zaien.aziz1605a@kecbu.uobaghdad.edu.iq)

Received: 1 September 2025, Revised: 11 September 2025, Accepted: 21 September 2025, Published: 10 December 2025

Abstract

This study presents the synthesis and application of a novel ZnO nanocatalyst doped with 10% Cu, prepared via a co-precipitation method, for the transesterification of waste cooking oil (WCO) into biodiesel. Comprehensive catalyst characterization was conducted using FT-IR, XRD, FE-SEM, EDS, AFM, BET, and HR-TEM. Process optimization was achieved through Response Surface Methodology (RSM) employing a Box-Behnken Design, which identified optimal conditions of 67 °C, 3.14 wt% catalyst, 47.47% methanol-to-oil ratio, and a reaction time of 90 min, yielding 95.5% biodiesel. Kinetic modeling revealed pseudo-first-order behavior with a relatively low activation energy of 99.3 kJ/mol. GC-MS analysis confirmed the dominance of C16:0, C18:1, and C18:0 methyl esters. Unlike previous works using undoped ZnO or CuO individually, this study demonstrates a synergistic effect of Cu-doping on ZnO that enhances catalytic activity and reduces activation energy. These findings highlight the efficacy of Cu-doped ZnO nanocatalysts for efficient and sustainable biodiesel production from low-grade feedstocks.

Keywords: Transesterification, Nanocatalyst, Waste cooking oil, Box-behnken design, Biodiesel, Activation energy

Introduction

Significant challenges confronting the world include finite fossil oil reserves and global warming, attributed to the escalating global energy consumption and the increase of atmospheric CO_2 from fossil fuel combustion [1]. The peak production capacity will be attained within this decade, subsequently leading to a decline in production. Consequently, there is an imperative necessity to identify a renewable energy resource that is clean, biodegradable, nontoxic, exhibits diminished emissions, possesses superior lubricating characteristics, is cost-effective, devoid of sulfur, and is economically viable [2,3]. Renewable energy fuels, such as biodiesel, are a viable approach to reducing the issues associated with fossil fuel consumption [4]. Due to the heightened awareness of environmental contamination concerns and the environmental impact is progressively increasing, resulting in numerous issues, including climate change and a decline in quality of life [5-7]. Recent life cycle assessment show that biodiesel made from oilseed crops, soybean/canola showing an estimated 40% - 69% reduction in CO_2 equivalents compared to petroleum diesel and out of waste-derived feedstock like UCO and animal tallow the reduction potential is higher of 79% - 86% under similar conditions [8]. The variety and accessibility of biofuel sources are critical aspects that promote the global exploration of biofuel utilization on a wide scale. Biomass has garnered significant interest as a source of renewable energy and platform chemicals [1,9]. The feedstock for biodiesel production is derived from local agriculture, indicating that biodiesel manufacturing occurs nationally [10,11]. One technique for creating biodiesels is the transesterification process, often known as the green process. The process creates esters by adding vegetable oils to an alcohol, usually methanol [12,13]. Notably, the byproduct of this process, glycerol, makes a significant contribution to cosmetics and medicinal science [14].

The utilization of nanotechnology and nanomaterials in biofuel research has emerged as a promising tool for providing cost-effective techniques to enhance fabrication properties [15]. Nanoparticles offer numerous advantages over traditional methods for biofuel production due to their size and unique properties [16-19], including an exceptional surface area-to-volume ratio and enhanced characteristics such as significant crystallinity, catalytic activity, adsorption capacity, and stability [20]. ZnO nanoparticles have become a successful catalyst for the production of biodiesel because of their special properties [1]. ZnO nanoparticles have stronger catalytic activity, greater stability, and reusability than other metal oxides like silicon dioxide (SiO_2) and titanium dioxide (TiO_2), while having a lower surface area-to-volume ratio, this problem can overcome by doping another metal [21,22]. Because of their enhanced catalytic activity, ZnO nanoparticles remain effective throughout a wide range of use cycles, lowering production costs overall [23].

The role of Cu doped ZnO nanoparticles in biodiesel production is thoroughly evaluated in this work, with a focus on technological developments, financial and environmental benefits, and scaling challenges [24]. While acknowledging existing constraints and outlining potential directions for future study, the goal is to fully evaluate the viability of using Cu-ZnO nanoparticles for large-scale biodiesel synthesis [24].

The need to lower production costs, manage lipid variability, cleanly dispose of used cooking oil, extend the lifespan of nanoparticles, and carefully evaluate studies are all examples of significant research gaps. By filling these gaps, the study aims to improve sustainable biodiesel production technology and support global efforts to reduce reliance on fossil fuels and promote the ideas of the circular economy [25-29]. The aim of the current study is to synthesis a novel catalyst Cu-doped ZnO nanoparticles and test how well they work as catalysts to produce biodiesel from waste cooking oil. The focus will be on improving the yield and quality of the fuel through the use of nanocatalysts and process modification.

Materials and methods

Materials

Zinc Sulfate Heptahydrate ($ZnSO_4 \cdot 7H_2O$) was supplied by Himedia, India with 99% purity, Copper(ll) Sulfate Pentahydrate ($CuSO_4 \cdot 5H_2O$) was supplied by Himedia, India with 99.5% purity, Sodium Carbonate (Na_2CO_3) was supplied by Loba Chemie, India with 99.5% purity were used as precursors. Phenolphthalein ($C_{22}H_{14}O_4$) used as Indicator. Methanol (CH_3OH) > 99% India, Potassium hydroxide (KOH) pellets was supplied by Himedia, India and Waste cooking oil from a restaurant for local fast food.

Preparation Cu-doped ZnO nanocatalyst

In the precent preparation, the precursors $ZnSO_4 \cdot 7H_2O$ and $CuSO_4 \cdot 5H_2O$ were first dissolved in 100 mL of distilled water in a beaker with 0.45 and 0.05 M to achieve 10% Cu-doped ZnO, mixed well on a magnetic hot plate with the magnetic bar, and the temperature was raised to 60 °C. In another beaker, a Na_2CO_3 solution (0.5 M) was progressively added dropwise under vigorous stirring (500 rpm) until the pH reached 8. Blue-White precipitates formed during 2 h of continuous stirring of the reaction mixture. After resting overnight, the final product was thoroughly washed 3 times using distilled water and ethanol to remove residual impurities and filtered, then placed in a hot air oven set to 80 °C for 2 h. A gemstone mortar was used for crushing the dry precursor into a fine powder. Finally, all hydroxide molecules are thermally decomposed by annealing the powdered products in a muffle furnace at 500 °C for 3 h.

$$_{(1-X)}ZnSO_4 \cdot 7H_2O + {}_xCuSo_4 \cdot 5H_2O + Na_2CO_3 \rightarrow Cu_xZn_{(1-x)}Co_3\downarrow + Na_2SO_4 + H_2O \quad (1)$$

After calcination at 500 °C for 3 h the product $Zn_{(1-x)}Cu_xCO_3$ was analyze as shown in following reaction:

$$Cu_xZn_{(1-x)}\,Co_3 \xrightarrow{\Delta 500\,^{\circ}C,\ 3\,h} Cu_xZn_{(1-x)}\,O + CO_2 \quad (2)$$

where x = 0.1 for 10% Cu doping and finally, the target product ($Cu_xZn_{(1-x)}O$) was saved in the desiccator in order to prevent it from moisture.

Catalyst characterization

The Cu-ZnO nanoparticles were characterized by using Fourier transform infrared (FT-IR) for functional group identification. The crystal structure was examined by X-ray Diffraction (XRD). The morphological and compositions characteristics of the Cu-doped ZnO nanoparticles were analyzed using field emission scanning electron microscopy (FE-SEM, EDS). Additional characterization of particles by Transmission Electron Microscopy (TEM). Furthermore, the surface topography and roughness of the nanoparticles were examined by Atomic Force Microscopy (AFM) and Brunauer-Emmett-Teller (BET) technique was used for specific surface area and porosity analysis. **Figure 1** shows the steps of synthesis of NPs catalysts and catalysts characterization.

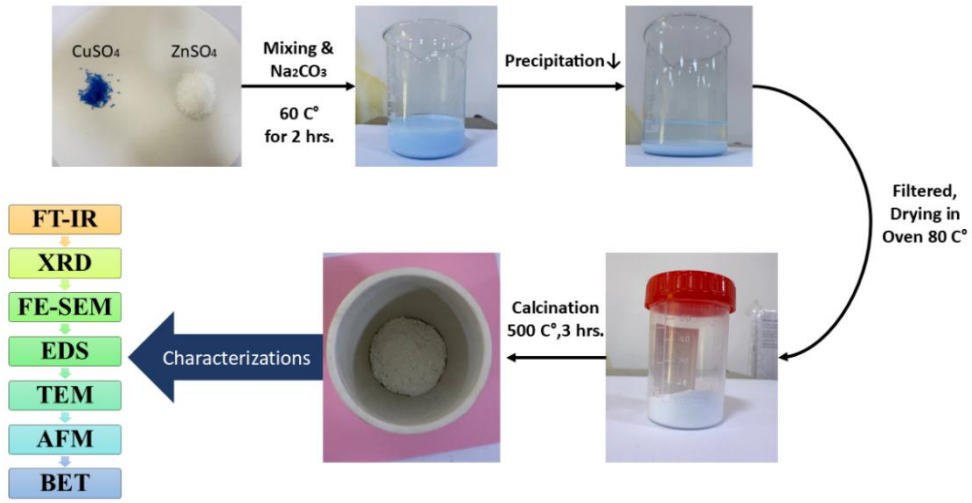

Figure 1 Schematic representation of the co-precipitation method for the synthesis of Cu-doped ZnO nanoparticles. $CuSO_4$ and $ZnSO_4$ precursors were mixed with Na_2CO_3 at 60 °C for 2 h.

Physicochemical analysis of WCO

A physicochemical analysis of waste cooking oil was conducted by assessing parameters like acid value, density, and saponification value. The density of waste oil was determined using the mass-to-volume formula. The acid value was determined by mixing 5 g of waste cooking oil with few drops of phenolphthalein indicator in a beaker. The beaker's contents were titrated with 0.01 N KOH until a pale pink hue appeared. The acid value of the oil was calculated utilizing the subsequent equation [30,31].

$$Acid\ value(AV) = \frac{KOH\ mL\ titrate \times N\ of\ KOH \times 56.1}{Weight\ of\ oil} \quad (3)$$

For the saponification value, 2 g of oil was measured and mixed with 25 mL of alcoholic KOH and a tiny amount of ethanol (3 mL). A reaction was performed with mixtures maintained at 100 °C for 1 h. Following incubation, they were allowed to cool, treated with phenolphthalein indicator, and then titrated with (0.5 N HCl). The saponification value of the waste oil was calculated using the specified equation [32].

$$Saponification\ value(SV) = \frac{Vol\ of\ HCL\ titrate \times 56.1 \times N\ of\ HCL}{Weight\ of\ oil} \quad (4)$$

Transesterification of waste cooking oil

Before transesterification process the waste cooking oil was filtrated through a cloth to remove the food residuals and then subject to heat at 120 °C, 2 h for removal of the moisture content, the treated oil was reacted with methanol in the present of Cu-ZnO as a catalyst. For each experiment, 20 g of pre-treated WCO were put into a 250 mL 3-nick round bottom flask connected with reflex condenser as shown in (**Figure 2**). Subsequently, a weight percentage of Cu-ZnO NPs catalyst ranging from 1% to 5% and methanol in a weight percentage ratio of 20 to 60 were incorporated into the oil. The reaction mixture was heated to a temperature range of 50 to 70 °C while being stirred at 600 r/min. The reaction mixture was subjected to reflux for a duration of 30 to 120 min. Ultimately the mixture

was subsequently transferred to a 250-mL separation funnel and allowed to stand for 12 - 24 h to achieve the distinct layers of biodiesel, glycerol, and catalyst [31].

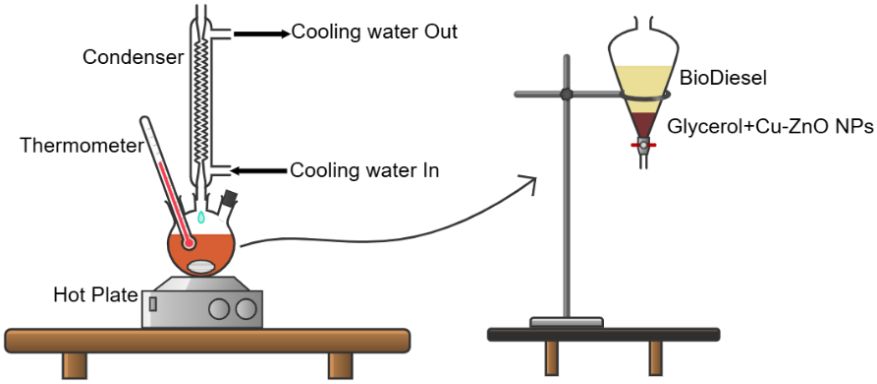

Figure 2 Experimental setup for biodiesel production via transesterification. The reaction was carried out in a 3 nick round bottom flask equipped with a reflux condenser and thermometer under constant stirring at 600 rpm.

Design of Experiments (DOE)

In the DOE, the factors use including alcohol, catalyst concentration, reaction time, and temperature. These factors are crucial to maximizing biodiesel yield from the transesterification process [33]. Consequently, the studies were executed utilizing a DOE in Minitab-21 statistical software, as illustrated in **Table 1**.

Table 1 Experimental range and level of process variables.

Biodiesel input	Low (-)	High (+)
Temperature °C	50	70
Catalyst %	1	5
Methanol to oil weight percent (M/O) %	20	60
Time (min)	30	120

The Response Surface Method (RSM) optimization strategy, utilizing Box-Behnken design, involved 27 experiments conducted randomly by varying the process variables in accordance with the Design of experiments. The experimental impacts of the response variables obtained from the maximum factorial design matrix were utilized to construct the quadratic response surface models. Relationships are established with the least squares method. In RSM, the input value is consistently represented as a numeric quantity [34,35].

In the current study, the Methanol to oil percent (M/O), Catalyst Concentration, Reaction Temperature, and Reaction Time were considered as input variables that possibly influence the production yield during biodiesel production. Experimental results according to Box-Behnken design-based Response Surface Methodology as shown in **Table 2**.

Table 2 Experimental design matrix and response values for biodiesel yield.

No.	Temperature	Catalyst	M/O ratio	Time(min)	Actual yield	Predict yield
1	60	3	40	75	92.31	92.54
2	60	3	20	30	67.00	67.53
3	50	3	60	75	70.33	70.25
4	70	3	40	120	89.71	90.39

No.	Temperature	Catalyst	M/O ratio	Time(min)	Actual yield	Predict yield
5	60	3	60	120	80.00	80.19
6	50	3	40	30	72.50	71.73
7	60	1	40	120	88.20	87.65
8	60	5	40	30	77.20	77.12
9	70	3	20	75	76.80	76.25
10	60	3	20	120	78.50	78.47
11	60	3	40	75	93.00	92.54
12	60	5	20	75	79.85	79.97
13	50	3	20	75	79.50	78.45
14	60	3	60	30	72.00	72.75
15	50	5	40	75	73.50	74.76
16	70	3	40	30	73.20	72.51
17	60	5	60	75	83.10	82.02
18	70	3	60	75	90.97	91.40
19	60	5	40	120	81.00	80.11
20	50	1	40	75	83.00	83.05
21	60	1	20	75	78.90	79.89
22	70	1	40	75	86.12	85.58
23	50	3	40	120	71.62	72.22
24	70	5	40	75	90.50	91.17
25	60	1	60	75	85.00	84.79
26	60	1	40	30	72.00	72.27
27	60	3	40	75	92.31	92.54

RSMs were used to optimize the process, and the most desirable solution was deemed to be the optimum one. The proper variables for the engine's operation are the variables that arise from the optimal solution. ANOVA, or analysis of variance, produces empirical data about potential advantages. The biodiesel yield was determined using the Eq. (5) [36].

$$Biodiesel\ yield\ \% = \frac{Weight\ of\ Biodiesel}{Weight\ of\ WCO} \times 100 \quad (5)$$

Reaction kinetics

In the transesterification reaction used test to find which kinetics to obey zero order, pseudo first order or second order. Orders rate constants were calculated by using Eqs. (6) - (8).

For 0 order [37];

$$X_A = Kt \quad (6)$$

For pseudo first order [37];

$$-ln(1 - X_A) = Kt \quad (7)$$

For second order [38];

$$\frac{X_A}{1-X_A} = Kt \quad (8)$$

where k denotes the rate constant, X_A represents yield at time. The Arrhenius equation, presented in the following equation, was utilized to determine the activation energy (Ea) for the transesterification processes [39].

$$ln\ K\ = -\frac{Ea}{RT} + ln\ P \quad (9)$$

where T signifies temperature, P symbolizes the pre-exponential factor, and R represents the gas constant, valued as 8.314×10^{-3} JK^{-1} mol^{-1}. The activation energy can be determined by plotting ln k against 1/T, which should yield a linear graph with a slope of -Ea/R [38].

Results and discussion

Characteristics of catalyst

Fourier Transform Infrared (FT-IR) spectroscopy

Fourier-transform infrared (FTIR) spectroscopy was conducted to investigate the functional groups and bonding characteristics of the synthesized Cu-doped ZnO nanoparticles. The FTIR spectrum as shown in (**Figure 3**) exhibited a broad absorption band around 3,410 cm^{-1}, which corresponds to the O-H stretching vibration of adsorbed moisture or surface hydroxyl groups [40]. A minor peak at 2,920 cm^{-1} is associated with C-H stretching, suggesting the presence of residual organic moieties from the synthesis process. The absorption band observed near 1,641 cm^{-1} is attributed to the bending vibration of O-H, further indicating adsorbed water molecules on the nanoparticle surface. Peaks located at 1452 and 1,371 cm^{-1} can be linked to C-H bending or sulphate groups, potentially originating from metal salt precursors [41]. Additionally, bands at 1,143 and 987 cm^{-1} suggest C-O stretching and possible metal-oxygen-metal (M-O-M) interactions [42]. Notably, a strong absorption peak around 418 cm^{-1} is characteristic of Zn-O or Cu-O stretching vibrations, confirming the formation of metal oxide bonds and validating the successful synthesis of Cu-doped ZnO nanoparticles [41,43]. These spectral features collectively confirm the presence of key functional groups and metal-oxygen bonding, essential for catalytic activity in applications such as biodiesel production.

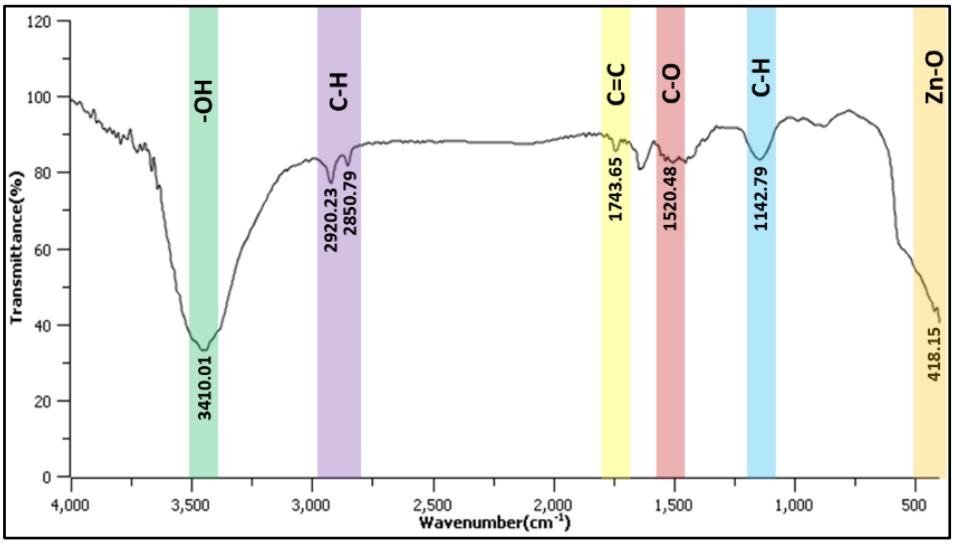

Figure 3 FT-IR spectrum of Cu-doped ZnO NPs showing key functional group.

X-ray Diffraction (XRD) spectroscopy

The crystalline structure of the Cu-doped ZnO nanoparticles was investigated using X-ray diffraction (XRD), and the resulting diffraction pattern is presented in (**Figure 4**). The spectrum shows a series of sharp, intense peaks, indicating a well-defined crystalline phase. The major diffraction peaks appear at 2θ values approximately corresponding to the (100), (002), (101), (102), (110), (103), and (112) planes, which are in good agreement with the standard hexagonal wurtzite structure of ZnO (JCPDS Card No. 36-1451) [44].

The absence of any secondary peaks associated with copper oxide (CuO or Cu_2O) or metallic Cu suggests that copper is likely incorporated into the ZnO lattice either substitutionally or interstitially, rather than forming separate crystalline phases [45]. This supports successful doping rather than simple mixing. The presence of peak broadening in the diffraction pattern further confirms the nanoscale crystallite size.

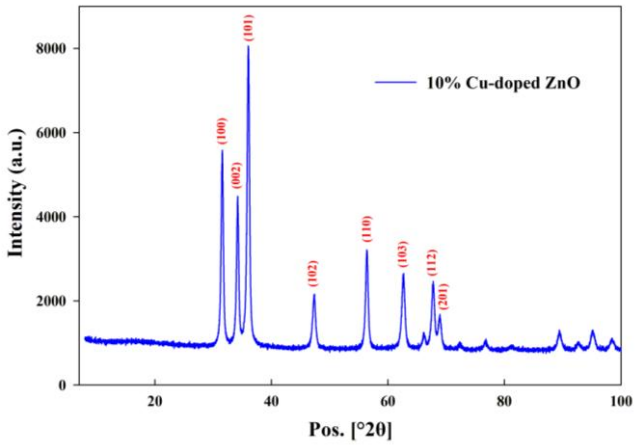

Figure 4 X-ray diffraction (XRD) pattern of 10% Cu-doped ZnO nanoparticles.

Using the Scherrer equation [46];

$$D = \frac{K\lambda}{\beta cos\theta} \quad (10)$$

where D is the crystallite size, K is the shape factor (typically 0.90 - 0.94), λ is the X-ray wavelength (commonly 0.15406 nm for Cu Kα) [47], β is the full width at half maximum (FWHM) in radians, and θ is the Bragg angle, the average crystallite size can be estimated if the FWHM data is available, average crystallite size is found to be 20 nm Based on the peak sharpness.

Field Emission Scanning Electron Microscopy (FE-SEM) and Energy Dispersive X-ray (EDX) spectroscopy

The morphological features of the produced Cu-doped ZnO nanoparticles were analyzed using Field Emission Scanning Electron Microscopy (FE-SEM) as shown in **Figure 5**. The micrographs demonstrate that the nanoparticles possess a significantly agglomerated and porous structure, consisting of irregular to quasi-spherical particles. The individual nanoparticles exhibited sizes ranging from around 40 to 45 nm, so validating their nanoscale dimensions [48]. (**Figure 6**) shows the elemental composition of the synthesized Cu-doped ZnO nanoparticles was investigated using Energy Dispersive X-ray Spectroscopy (EDX).

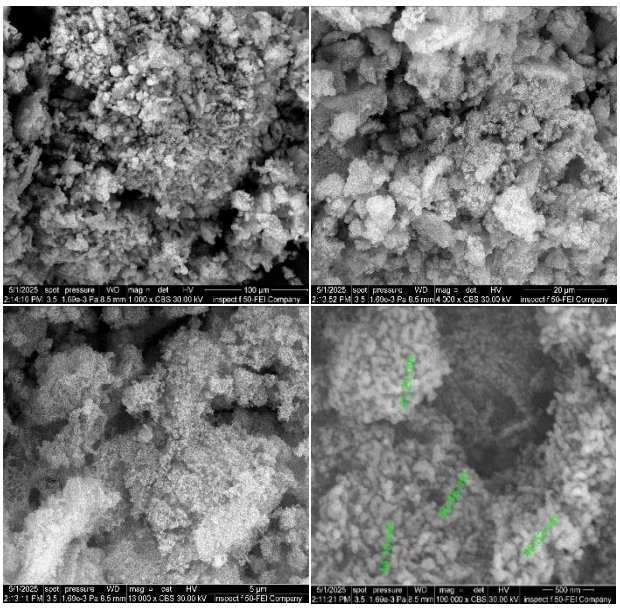

Figure 5 FE-SEM of Cu-doped ZnO NPs at Different Magnification (100 µ, 20 µ, 5 µ and 500 nm).

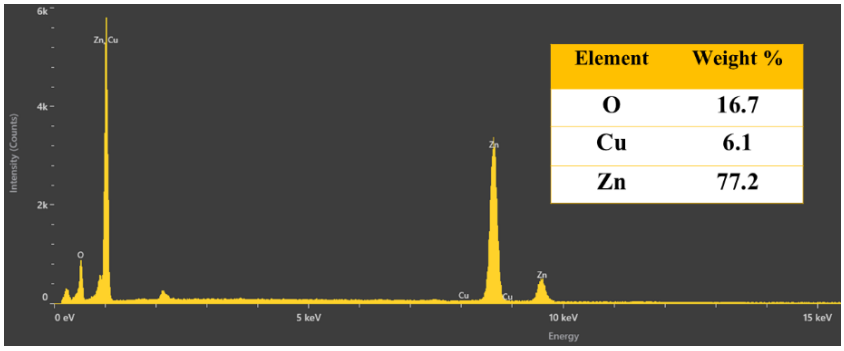

Figure 6 EDX spectrum along with quantified element composition table.

Atomic Force Microscopy (AFM)

The surface morphology of the synthesized catalyst was studied in a 2.5×2.5 μm^2 area. The 3D and deflection photos showed that the surface was not smooth and had a lot of rises and drops (**Figures 8(a)** and **8(b)**). These results show that a nanostructured surface with a rather large surface area has formed, which is beneficial for improving catalytic effectiveness in related uses as a catalyst in biodiesel production [49].

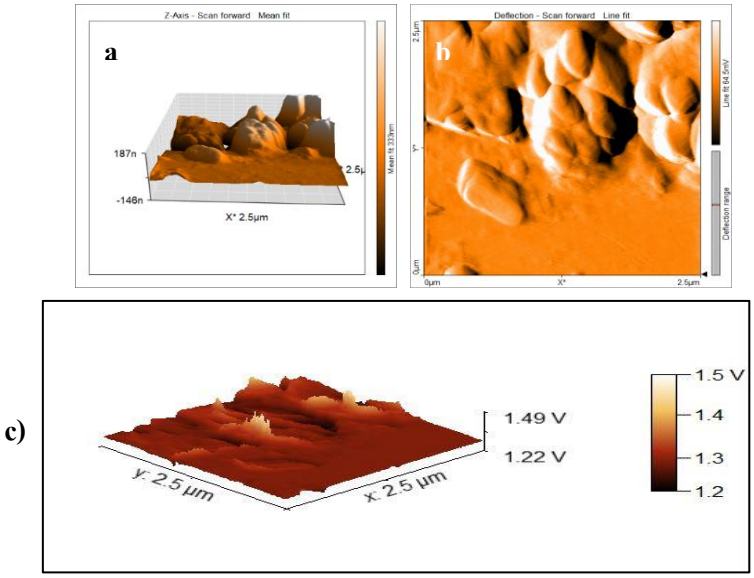

Figure 7 Atomic force microscopy (AFM) analysis of Cu-doped ZnO NPs: (a) 3D surface topography, (b) deflection image in scan forward mode, (c) voltage distribution mapping.

High-Resolution Transmission Electron Microscopy (HR-TEM)

The TEM image (**Figure 8(a)**) shows that the Cu-doped ZnO nanoparticles are roughly spherical and agglomerated, with individual particle sizes generally in the range of 10 - 30 nm. The observed aggregation may be attributed to the high surface energy of the nanoparticles, which is common in metal oxide nanostructures.

The Selected Area Electron Diffraction (SAED) pattern (**Figure 8(b)**) displays a series of well-defined concentric rings, indicating the polycrystalline nature of the sample. These diffraction rings correspond to the characteristic lattice planes of the wurtzite hexagonal structure of ZnO, with minor shifts or intensity changes likely due to the substitution of Zn^{2+} ions with Cu^{2+} ions in the crystal lattice. The presence of sharp and discrete spots superimposed on the rings further suggests the presence of nanocrystalline domains within the agglomerates.

The HR-TEM image (**Figure 8(c)**) reveals clear lattice fringes with interplanar spacings consistent with those of the ZnO wurtzite phase. The observed lattice fringe spacing (~0.26 nm) corresponds to the (002)

plane of ZnO. Localized distortion of lattice planes may be indicative of Cu doping, which introduces strain and defects due to the difference in ionic radii between Zn^{2+} and Cu^{2+} ions. No distinct secondary phase or segregation of CuO or metallic Cu was observed, suggesting successful incorporation of Cu into the ZnO lattice at the atomic level.

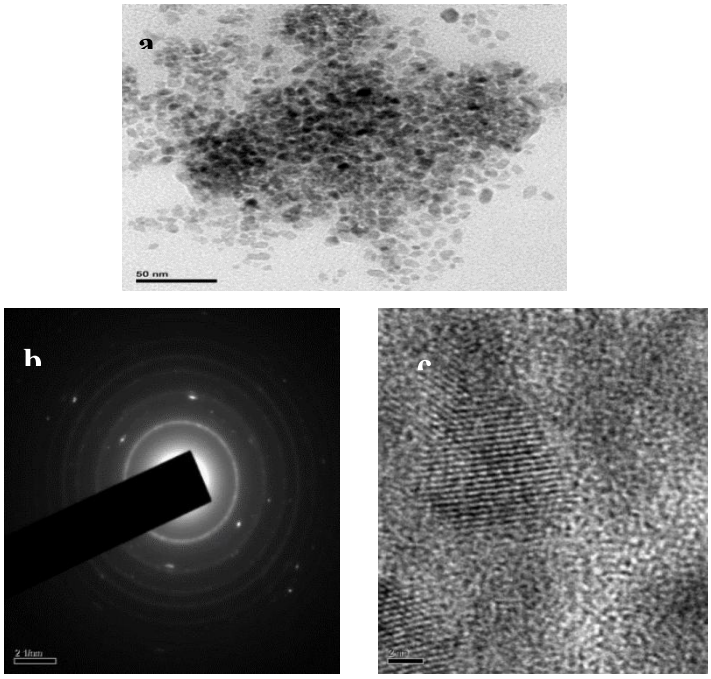

Figure 8 (a) Transmission Electron Microscopy (TEM), (b) The SAED pattern and (c) High-Resolution Transmission Electron Microscopy (HR-TEM).

Brunauer-Emmett-Teller (BET)

The BET method is a widely used technique for determining the average pore diameter, isotherm sorption of nitrogen, total pore volume, and specific surface area of the synthesized Cu-doped ZnO nanocatalyst [50,51], as shown in **Figures 9(a)** and **9(b)**. The N_2 sorption isotherm displayed a type IV curve with a hysteresis loop, conforming the mesoporous structure of Cu doped ZnO NPs. The nanocatalysts significant surface area of 59.534 m^2g^{-1} with average pore volume 0.2392 cm^3g^{-1} and average pore diameter 24.141 nm is a crucials aspect for catalysis. Enhanced surface area provides more Lewis acidic sites (Zn^{2+}) and basic sites (O^{2-}, Cu^{2+} substitution), which are required for methanol activation and triglyceride cleavage. This explains why Cu-ZnO catalysts often outperform pure ZnO in biodiesel yield. Scientific literature emphasises the significance of elevated surface area in catalysis. The literature indicates that an increased surface area offers a higher quantity of active sites for catalytic processes [50].

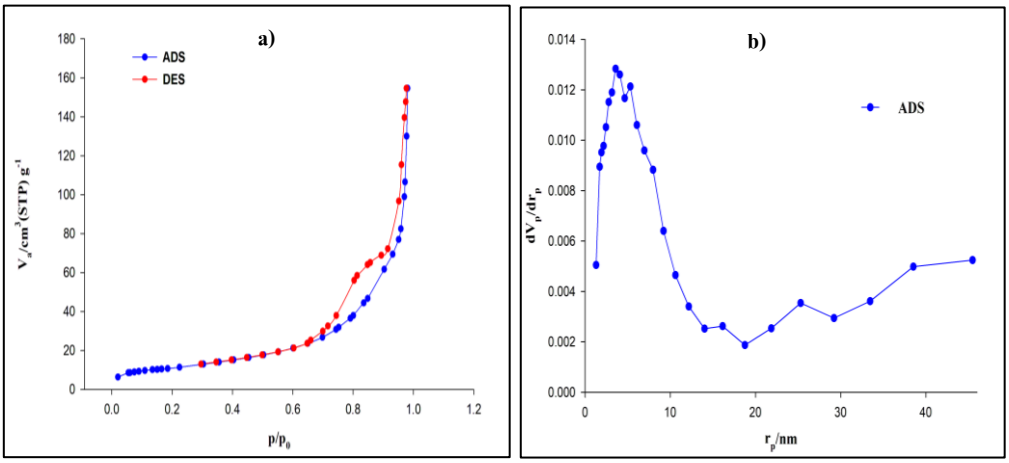

Figure 9 (a) The N_2 adsorption-desorption isotherm of Cu doped ZnO. (b) Distribution of pore size.

Characteristics of waste cooking oil

The characteristics of feedstock indicate the quality of biodiesel. The physical parameters of pre-treated waste cooking oil are quantified, and the results are presented in the (**Table 3**).

Table 3 Physical parameters of waste cooking oil.

No.	Properties	Measured Values
1	Density	931.3 kg/m^3
2	Kinematic Viscosity	39 mm^2/s
3	Acid Value	1.6 mg KOH/g
4	Flash Point	283 °C
5	Saponification Value	193 mg KOH/g
6	Pour Point	−13.5 °C
7	Iodine Value	112 g I_2/100g

Modeling results and data analysis utilizing (RSM)

Experimental data derived from Box-Behnken design (BBD) were utilized to ascertain the optimal combination of several operating parameters (including temperature, methanol/oil percent ratio, time, and catalyst concentration) to maximize biodiesel production.

Advanced multiple regression analysis was applied to the experimental data to derive a second-order polynomial equation with regression coefficients, which were subsequently evaluated for statistical significance [52,53]. The biodiesel yield from waste cooking oil varied between 67% and 93% based on laboratory experiments. The model's projected second-order polynomial equation for maximal biodiesel is presented in Eq. (11).

$$Biodiesel\ Yield\ \%(Y) = -86.7 + 4.948\,A - 2.71\,B + 0.006\,C + 0.4121\,D - 0.05739\,A^2 - 0.790\,B^2 - 0.01928\,C^2 - 0.004983\,D^2 + 0.1735\,AB + 0.02918\,AC + 0.00966\,AD - 0.0178\,BC - 0.03444\,BD - 0.000972\,CD \quad (11)$$

where A is the temperature (°C), B is the catalyst loading (wt.%), C is the methanol to oil ratio (wt.%), and D is the reaction time (min).

In **Table 4** shows the results of an analysis of variance (ANOVA) that looked at the statistical significance of the process variables that affect biodiesel yield. The significance of individual process variables and their interactions on biodiesel yield was evaluated using analysis of variance (ANOVA). The model exhibited a highly significant F-value of 127.72 ($p < 0.0001$), indicating strong predictive capability and a good fit to the experimental data [54]. Among the linear terms, reaction temperature, methanol-to-oil (M/O)

ratio, and reaction time had highly significant effects ($p < 0.0001$), whereas the catalyst amount was moderately significant ($p = 0.028$). Quadratic effects were also prominent, with all squared terms (Temp^2, Catalyst^2, M/O ratio^2, and Time^2) showing p-values less than 0.0001, highlighting notable curvature in the response surface.

Furthermore, several 2-way interactions were statistically significant, including Temp*Catalyst, Temp*M/O ratio, Temp*Time, and Catalyst*Time, all with p-values below 0.0001. This implies synergistic effects between these variables significantly influence biodiesel conversion. In contrast, the interactions Catalyst*M/O ratio and M/O ratio*Time were not significant ($p = 0.152$ and 0.082, respectively), suggesting minimal interactive influence.

The model's lack-of-fit was not significant ($p = 0.143$), confirming that the model adequately describes the experimental data without substantial unexplained variation. Additionally, the low pure error indicates good repeatability of the experimental runs. Overall, the ANOVA results confirm that the selected quadratic model is robust and appropriate for optimizing biodiesel production using Cu-doped ZnO nanocatalysts.

Table 4 Analysis of variance (ANOVA).

Source	DF	Adj SS	Adj MS	F-Value	*p*-Value
Model	14	1,550.96	110.783	127.72	0.0001
Linear	4	564.26	141.064	162.63	0.0001
A-Temp	1	269.33	269.327	310.5	0.0001
B-Catalyst	1	5.43	5.428	6.26	0.0280
C-M/O ratio	1	36.22	36.223	41.76	0.0001
D-time	1	253.28	253.276	292	0.0001
Square	4	683.22	170.805	196.92	0.0001
A^2	1	175.64	175.641	202.49	0.0001
B^2	1	53.3	53.301	61.45	0.0001
C^2	1	317.35	317.351	365.87	0.0001
D^2	1	543.11	543.107	626.14	0.0001
2-Way Interaction	6	303.49	50.582	58.31	0.0001
AB	1	48.16	48.164	55.53	0.0001
AC	1	136.19	136.189	157.01	0.0001
AD	1	75.6	75.603	87.16	0.0001
BC	1	2.03	2.032	2.34	0.1520
BD	1	38.44	38.44	44.32	0.0001
CD	1	3.06	3.062	3.53	0.0850
Error	12	10.41	0.867		
Lack-of-Fit	10	10.09	1.009	6.36	0.1430
Pure Error	2	0.32	0.159		
Total	26	1,561.37			
Model summary	$R^2 = 99.33\%$		R^2(adj) = 98.56%	R^2(pred) = 96.23%	S = 0.931

Effects of process input variables on biodiesel production

The influence of independent factors (M/O percent ratio, catalyst loading, temperature, and reaction time) on the experimental biodiesel yield was examined by 3D surface plots as shown in (**Figure 10**). The interaction between 2 variables in the model graphs can be observed

while maintaining other parameters at their central values.

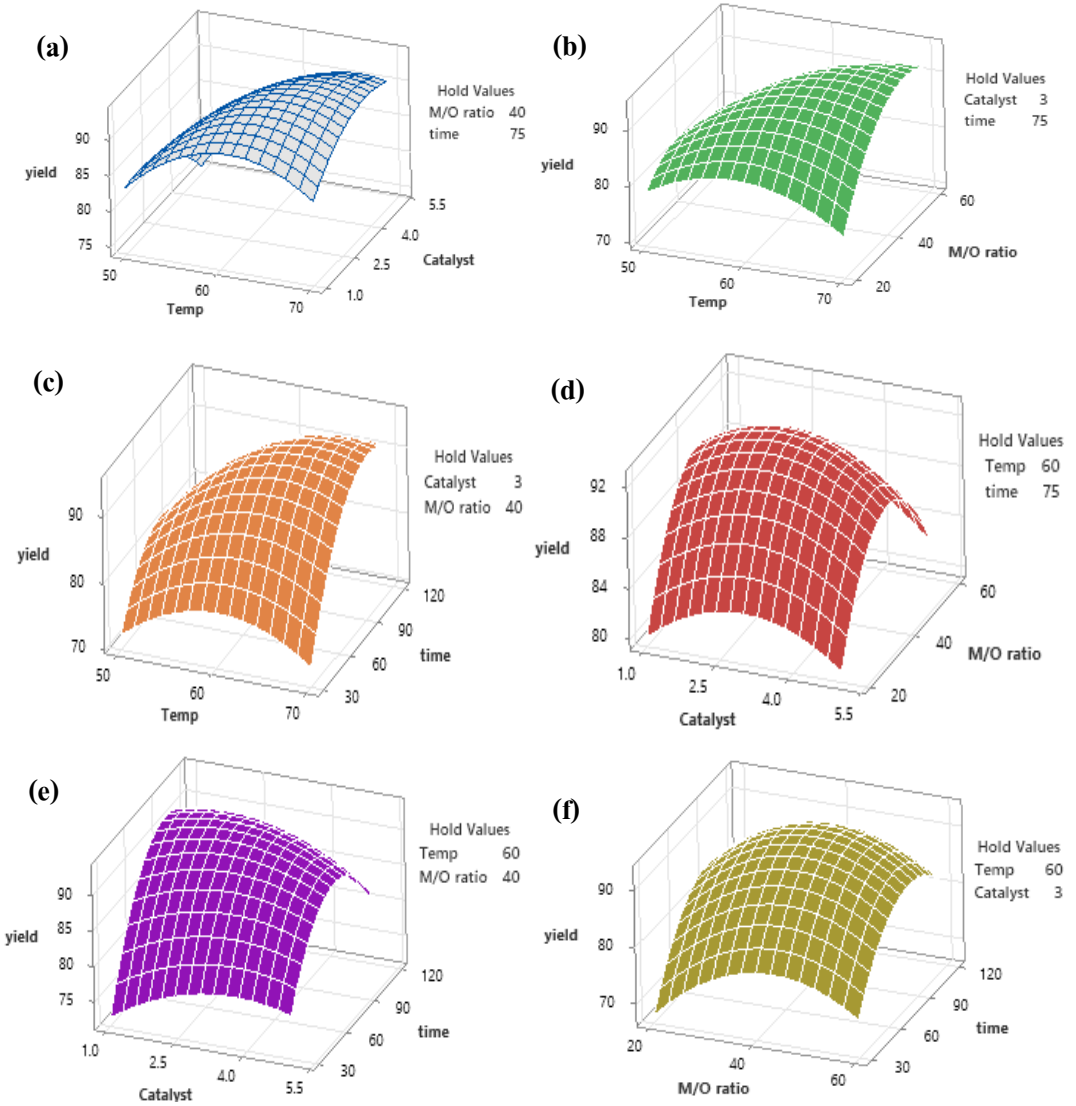

Figure 10 Response surface plots the interaction effects of (a) catalyst and temperature, (b) methanol amount and temperature, (c) time and temperature, (d) methanol amount and catalyst, (e) catalyst and time (f) time and methanol amount.

Response optimization: Yield

The used response surface methodology (RSM) to find the best transesterification process parameters for making biodiesel with Cu-doped ZnO nanoparticles as a catalyst. According to the model as shown in (**Figure 11**) the best conditions were a temperature of 67.57 °C, a catalyst loading of 3.14 wt%, an M/O weight percent of 47.47%, and a reaction duration of 90.9 min. The expected maximum biodiesel yield was 95.5% under these conditions, and the desirability value was 1.000, which means that the optimization goal was met quite well. The curved lines on the response plots show that process variables interact with each other in a nonlinear way, which proves that RSM is good at finding the most important components. These results show that Cu-doped ZnO nanoparticles are very good at catalyzing reactions and might be used to improve biodiesel production by changing the right parameters.

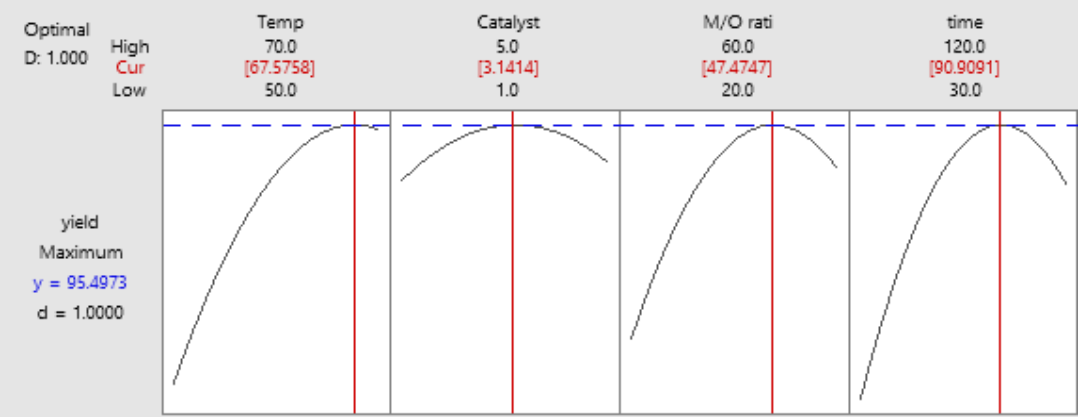

Figure 11 Optimization profile plots of process variables affecting biodiesel yield using RSM.

Kinetic study

Zero order, Pseudo 1st order and 2nd order models were applied to correlate the kinetics data. Parameters for each model were established by fitting the linearized forms of these models to a set of experimental data, as shown in (**Figure 12**). Which demonstrates a fair agreement and their constant are presented in (**Table 5**). Based on correlation coefficients, pseudo-first-order kinetic model provides better representation for the biodiesel production, these findings are in agreement with those reported by Gurunathan and Ravi [55]; Hazrat *et al.* [55]; Hazrat *et al.* [57]. The kinetic studies of the transesterification of WCO catalyzed by Cu-doped ZnO nanocatalyst were conducted for a duration of 30 to 90 min. Kinetic investigations of the reaction were conducted at 50, 55, 60 and 65 °C, as the rate constant is dependent on the reaction temperature [58].

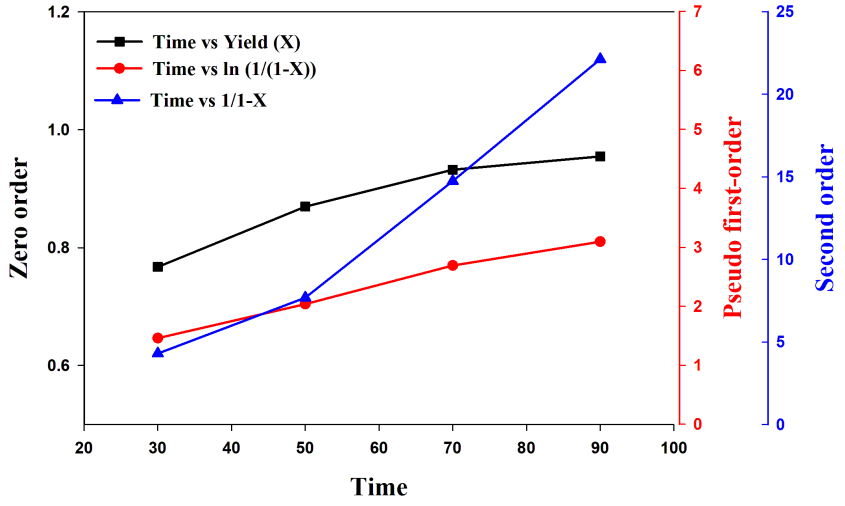

Figure 12 Reaction order fitting for transesterification: Yield vs. time for various kinetic models.

Table 5 Comparison of kinetic parameters for 0, pseudo-first, and second order models.

Order of reaction	K(min^{-1})	R^2
Zero order	0.0031	0.92
Pseudo first order	0.0278	0.99
Second order	0.3028	0.97

Activation energy of Cu-doped ZnO nano catalysts was calculated using Arrhenius equation [59,60], which is presented in **Table 6**. **Figure 13** shows the plot of ln k and 1/T. Therefore, the activation energy

of Cu-doped ZnO catalyzed transesterification was 99.3356 kJ/mol.

Table 6 Kinetic data for Arrhenius plot of Cu-doped ZnO catalyzed transesterification.

Temperature (°C)	Temp (K)	Constant rate (K)	Ln (K)	1/T (k)
50	323.15	0.005	−5.29831737	0.00309
55	328.15	0.0105	−4.55638002	0.00305
60	333.15	0.0179	−4.02295457	0.003
65	338.15	0.0258	−3.65738079	0.00296

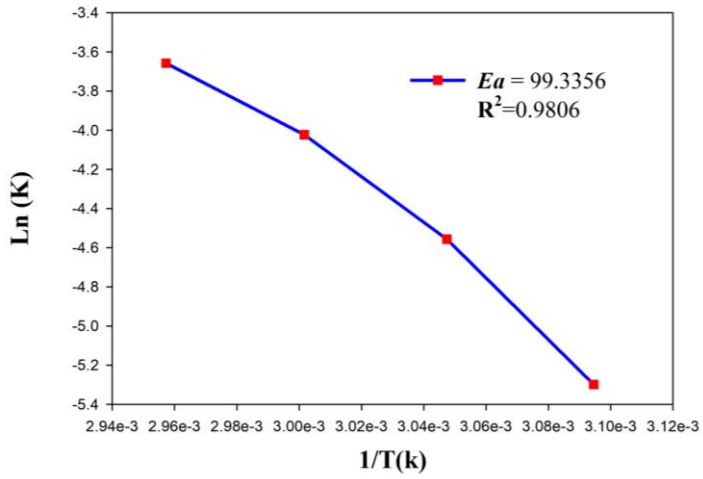

Figure 13 Arrhenius plot of Ln(k) versus 1/T (K) for the transesterification reaction using Cu-doped ZnO nanocatalyst.

Gas chromatography-mass spectrometry analysis

GC-MS analyses facilitate the identification of the chemical composition of the biodiesel [61], as illustrated in (**Figure 14**). **Table 7** confirmed the presence of several fatty acid methyl ester composition in WCO biodiesel as determined by the GC-MS method. The GC-MS analytical report identified the principal FAMEs as Methyl palmitate (C16:0), Methyl oleate (C18:1) and Methyl stearate (C18:0), which exhibited significant peaks. These compounds collectively accounted for over 99% of the total peak area. In contrast minor peaks in GC-MS analysis, such as methyl butanoate, are likely artifacts or trace intermediates generated during the transesterification process, not significant contributors to biodiesel composition or quality, and do not affect the overall fuel assessment, which is primarily based on long-chain FAMEs [62].

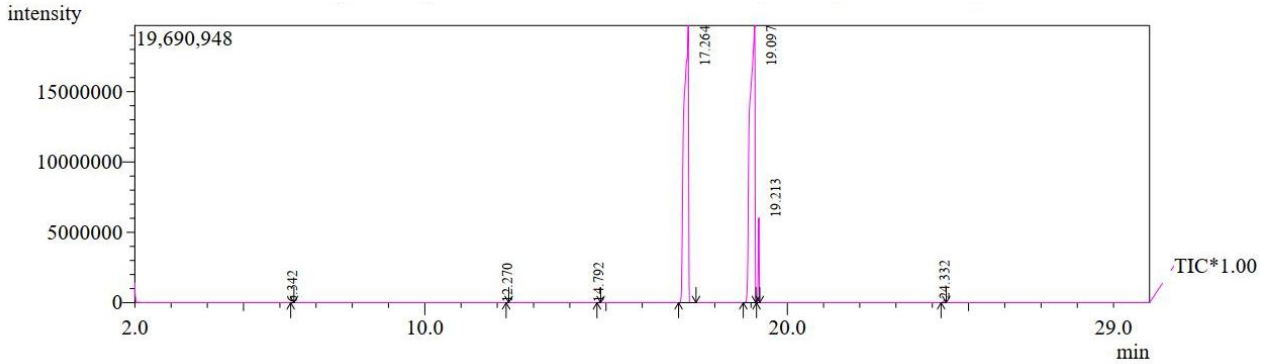

Figure 14 The GC-MS of Waste cooking oil biodiesel.

Table 7 Principal compounds detected in GC-MS analysis.

Peak	Retention Time (min)	Compound Name	Identified Compound	Molecular Formula	Molecular Weight (g/mol)	Area (%)
1	6.34	Butyric acid methyl ester	Methyl butanoate	$C_5H_{10}O_2$	102	0.01
2	12.27	Butyric acid methyl ester	Methyl butanoate	$C_5H_{10}O_2$	102.13	0.001
3	14.79	Methyl tetradecanoate	Methyl myristate	$C_{15}H_{30}O_2$	242	0.02
4	17.26	Hexadecanoic acid methyl ester	Methyl palmitate ($C_{16:0}$)	$C_{17}H_{34}O_2$	270	45.8
5	19.1	Octadecenoic acid methyl ester	Methyl oleate ($C_{18:1}$)	$C_{19}H_{36}O_2$	296	51.39
6	19.21	Octadecenoic acid methyl ester	Methyl stearate ($C_{18:0}$)	$C_{19}H_{38}O_2$	298	2.63
7	24.33	Monoglyceride of linoleic acid	Glyceryl monooleate (monoglyceride)	$C_{21}H_{40}O_4$	356	0.15

Scalability considerations

Despite a high biodiesel yield (95.5%) together with good kinetic results obtained at the laboratory-scale, possible limitations in terms of scale-up are needed to be evaluated. Recovery and re-use of the catalyst is significant to reduce the cost and the waste of the material. Nanoparticle off-loading may be technically challenging which has process feasibility (in continuous processes) implications. In addition to performance, the cost of catalyst preparation and its impact on the $/L biodiesel price should also be compared to determine the commercial competitiveness. It will be necessary to address this in future studies to verify the industrial applicability of Cu-ZnO catalysts.

Conclusions

The current work has effectively documented the application of a 10% copper-doped zinc oxide catalyst for the transesterification of waste cooking oil. An affordable, biodegradable, and environmentally friendly nanocatalyst produced by the co-precipitation approach was employed in the synthesis of biodiesel from inexpensive and readily available oil. The synthesized catalyst was extensively characterized utilizing FT-IR, XRD, FE-SEM, EDX, AFM, TEM and BET techniques. Furthermore, GC-MS was employed to characterize the synthesized biodiesel. The optimal operational parameters were determined to be a temperature of 67 °C, a reaction time period 90 min, a methanol to waste cooking oil weight ratio of 47.47%, a catalyst loading of 3.14 wt.%, and a stirring speed of 600 rpm, resulting in a biodiesel yield of 95.5%.Consequently, the production of biodiesel from waste cooking oil under optimum conditions might be considered a viable feedstock to potentially substitute Petro-diesel fuel in existing engines and meet the growing need for fuel oil.

Acknowledgements

The authors express their sincere gratitude to the University of Baghdad, Al-Khwarizmi College of Engineering, Department of Biochemical Engineering, Iraq for providing laboratory facilities, technical assistance, and continuous support throughout this research.

Declaration of Generative AI in Scientific Writing

The authors acknowledge the use of generative AI tools (e.g., QuillBot and ChatGPT by OpenAI) in the preparation of this manuscript, specifically for language editing and grammar correction. No content generation or data interpretation was performed by AI. The authors

take full responsibility for the content and conclusions of this work.

CRediT author statement

Zain A. Sayhood: Conceptualization; Methodology; Software; Data curation; Writing - Original draft preparation. **Ziad T. Alismaeel:** Supervision; Visualization; Writing - Reviewing and Editing; Investigation.

References

[1] SM Salim, R Izriq, MM Almaky and AA Al-Abbassi. Synthesis and characterization of ZnO nanoparticles for the production of biodiesel by transesterification: Kinetic and thermodynamic studies. *Fuel* 2022; **321**; 124135.

[2] F Almomani, A Abdelbar and S Ghanimeh. A review of the recent advancement of bioconversion of carbon dioxide to added value products: A state of the art. *Sustainability* 2023; **15(13)**, 10438.

[3] K Sunilkumar, N Edayadulla, P Raja and R Surakasi. *The effect of emissions from DI-based sources causing hazardous health effects. In*: S Sahoo and N Yedla (Eds.). Recent advances in mechanical engineering. Springer, Singapore, 2024, p. 1-13.

[4] GC Manjunath Patel, BS Ajith, Jagadish, AK Shettigar and OD Samuel. *Introduction to renewable energy resources and sustainable feedstocks for biodiesel. In*: GC Manjunath Patel, BS Ajith, Jagadish, AK Shettigar and OD Samuel (Eds.). Biofuel production, performance, and emission optimization. Springer, Cham, Switzerland, 2025, p. 1-21.

[5] D Neupane. Biofuels from renewable sources, a potential option for biodiesel production. *Bioengineering* 2022; **10(1)**, 29.

[6] KS Kumar and S Muniamuthu. Assessment of performance, combustion, and emission characteristics of single cylinder diesel engine fuelled by pyrolysis oil + CeO_2 nanoparticles and 1-butanol blends. *International Journal of Ambient Energy* 2024; **45(1)**, 2344568.

[7] K Sunil Kumar, JM Babu and H Venu. Performance, combustion and emission characteristics of a single-cylinder DI diesel engine fuelled with lotus biodiesel-diesel- n - butanol blends. *International Journal of Ambient Energy* 2022; **43(1)**, 7941-7951.

[8] H Xu, L Ou, Y Li, TR Hawkins and M Wang. Life cycle greenhouse gas emissions of biodiesel and renewable diesel production in the United States. *Environmental Science & Technology* 2022; **56(12)**, 7512-7521.

[9] KS Kumar and S Muniamuthu. Design and fabrication of nickel-chromium reinforced 2-stage energy efficient pyrolysis reactor for waste plastics applications. *International Journal of Ambient Energy* 2024; **45(1)**, 2288148.

[10] A Singh and T Mukherjee. Application of carotenoids in sustainable energy and green electronics. *Materials Advances* 2022; **3(3)**, 1341-1358.

[11] ZT Alismaeel, TM Al-Jadir, TM Albayati, AS Abbas and AM Doyle. Modification of FAU zeolite as an active heterogeneous catalyst for biodiesel production and theoretical considerations for kinetic modeling. *Advanced Powder Technology* 2022; **33(7)**, 103646.

[12] A Karadağ, ÖD Şahan, A Hamid and MN Aftab. *Biodiesel production potential in sustainable biomass diversity. In*: E Jacob-Lopes, LQ Zepka and M Deprá (Eds.). Biodiesel plants - fueling the sustainable outlooks. IntechOpen, London, 2024.

[13] AE Atabani, AS Silitonga, HC Ong, TMI Mahlia, HH Masjuki, IA Badruddin and H Fayaz. Non-edible vegetable oils: A critical evaluation of oil extraction, fatty acid compositions, biodiesel production, characteristics, engine performance and emissions production. *Renewable and Sustainable Energy Reviews* 2013; **18**, 211-245.

[14] V Gupta and KP Singh. The impact of heterogeneous catalyst on biodiesel production; a review. *Materials Today: Proceedings* 2023; **78**, 364-371.

[15] AB Rashid. Utilization of nanotechnology and nanomaterials in biodiesel production and property enhancement. *Journal of Nanomaterials* 2023; **2023(1)**, 7054045.

[16] A Singh, A Gangwar and S Kumar. Prospects and limitations of existing biofuels and emerging trends in the utilization of nanoparticles for

enhanced biofuel production and microbial fuel cell efficiency. *Biofuels* 2025; **16(5)**, 519-544.

[17] KS Kumar, R Surakasi, SGK Patro, N Govil, MK Ramis, A Razak, P Sharma, M Alsubih, S Islam, TMY Khan, N Almakayeel and S Chintakindi. Performance, combustion, and emission analysis of diesel engine fuelled with pyrolysis oil blends and n-propyl alcohol-RSM optimization and ML modelling. *Journal of Cleaner Production* 2024; **434**, 140354.

[18] KS Kumar, JM Babu, H Venu and A Muthuraja. Waste plastic as a source of biofuel for stationary diesel engine: A critical review. *International Journal of Ambient Energy* 2022; **43(1)**, 8577-8591.

[19] D Bouras, M Fellah, R Barille, M Abdul Samad, M Rasheed and MA Alreshidi. Properties of MZO/ceramic and MZO/glass thin layers based on the substrate's quality. *Optical and Quantum Electronics* 2024; **56(1)**, 104.

[20] M Rozan, E Alamri and H Bayomy. Fermented Hass avocado kernel: Nutritional properties and use in the manufacture of biscuits. *Saudi Journal of Biological Sciences* 2022; **29(6)**, 103295.

[21] O Awogbemi, AA Ojo and SA Adeleye. Advancements in the application of metal oxide nanocatalysts for sustainable biodiesel production. *Discover Applied Sciences* 2024; **6(5)**, 250.

[22] I Alshalal, HMI Al-Zuhairi, AA Abtan, M Rasheed and MK Asmail. Characterization of wear and fatigue behavior of aluminum piston alloy using alumina nanoparticles. *Journal of the Mechanical Behavior of Materials* 2023; **32(1)**, 20220280.

[23] N Dey, S Vickram, S Thanigaivel, R Subbaiya, W Kim, N Karmegam and M Govarthanan. Nanomaterials for transforming barrier properties of lignocellulosic biomass towards potential applications - A review. *Fuel* 2022; **316**, 123444.

[24] RS Gavhane, AM Kate, A Pawar, MEM Soudagar and H Fayaz. Effect of soybean biodiesel and copper coated zinc oxide nanoparticles on enhancement of diesel engine characteristics. *Energy Sources, Part A: Recovery, Utilization, and Environmental Effects* 2025; **47(1)**, 3547-3565.

[25] M Guo, W Jiang, C Chen, S Qu, J Lu, W Yi and J Ding. Process optimization of biodiesel production from waste cooking oil by esterification of free fatty acids using La^{3+}/ZnO-TiO_2 photocatalyst. *Energy Conversion and Management* 2021; **229**, 113745.

[26] MA Sarhan, S Shihab, BE Kashem and M Rasheed. New exact operational shifted pell matrices and their application in astrophysics. *Journal of Physics: Conference Series* 2021; **1879(2**), 022122.

[27] D Bouras, M Rasheed, R Barille and MN Aldaraji. Efficiency of adding DD3+(Li/Mg) composite to plants and their fibers during the process of filtering solutions of toxic organic dyes. *Optical Materials* 2022; **131**, 112725.

[28] M Rasheed, MN Al-Darraji, S Shihab, A Rashid and T Rashid. Solar PV modelling and parameter extraction using iterative algorithms. *Journal of Physics: Conference Series* 2021; **1963(1)**, 012059.

[29] S Shihab, M Rasheed, O Alabdali and AA Abdulrahman. A novel predictor-corrector hally technique for determining the parameters for nonlinear solar cell equation. *Journal of Physics: Conference Series* 2021; **1879(2)**, 022120.

[30] Y Wang, SOP Liu and Z Zhang. Preparation of biodiesel from waste cooking oil via 2-step catalyzed process. *Energy Conversion and Management* 2007; **48(1)**, 184-188.

[31] ZT Alismaeel, AS Abbas, TM Albayati and AM Doyle. Biodiesel from batch and continuous oleic acid esterification using zeolite catalysts. *Fuel* 2018; **234**, 170-176.

[32] B Sajjadi, AAA Raman and H Arandiyan. A comprehensive review on properties of edible and non-edible vegetable oil-based biodiesel: Composition, specifications and prediction models. *Renewable and Sustainable Energy Reviews* 2016; **63**, 62-92.

[33] SE Onoji, SE Iyuke, AI Igbafe and MO Daramola. Transesterification of rubber seed oil to biodiesel over a calcined waste rubber seed shell catalyst: modeling and optimization of process variables. *Energy & Fuels* 2017; **31(6)**, 6109-6119.

[34] HS Pali, A Sharma, N Kumar and Y Singh. Biodiesel yield and properties optimization from Kusum oil by RSM. *Fuel* 2021; **291**, 120218.

[35] KS Kumar, A Razak, A Yadav, PSR Rao, HS Majdi, TMY Khan, N Almakayeel and K Singh. Experimental analysis of cycle tire pyrolysis oil doped with 1-decanol + TiO_2 additives in compression ignition engine using RSM optimization and machine learning approach. *Case Studies in Thermal Engineering* 2024; **61**, 104863.

[36] DYC Leung and Y Guo. Transesterification of neat and used frying oil: Optimization for biodiesel production. *Fuel Processing Technology* 2006; **87(10)**, 883-890.

[37] A Monyem, JH Van Gerpen and M Canakci. The effect of timing and oxidation on emissions from biodiesel-fueled engines. *Transactions of the ASAE* 2001; **44(1)**, 35-42.

[38] HM Mahmudul, FY Hagos, R Mamat, AA Adam, WFW Ishak and R Alenezi. Production, characterization and performance of biodiesel as an alternative fuel in diesel engines - A review. *Renewable and Sustainable Energy Reviews* 2017; **72**, 497-509.

[39] Y Yang, M Jiang, L Song, Y Shen, T Lei and J Cai. Systematical analysis and application of distributed activation energy model (DAEM) with Weibull distribution for pyrolysis kinetics of lignocellulosic biomass. *Renewable Energy* 2024; **237**, 121549.

[40] D Kumbhar, S Kumbhar, S Delekar, R Nalawade and A Nalawade. Photoelectrochemical cell performance Cu doped ZnO photoanode sensitized by xanthene dyes. *Nanosystems: Physics, Chemistry, Mathematics* 2019; **10(4)**, 466-474.

[41] S Muthukumaran and R Gopalakrishnan. Structural, FTIR and photoluminescence studies of Cu doped ZnO nanopowders by co-precipitation method. *Optical Materials* 2012; **34(11)**, 1946-1953.

[42] PK Labhane, VR Huse, LB Patle, AL Chaudhari and GH Sonawane. Synthesis of Cu doped ZnO nanoparticles: Crystallographic, optical, FTIR, morphological and photocatalytic study. *Journal of Materials Science and Chemical Engineering* 2015; **03(7)**, 39-51.

[43] S Singhal, J Kaur, T Namgyal and R Sharma. Cu-doped ZnO nanoparticles: Synthesis, structural and electrical properties. *Physica B: Condensed Matter* 2012; **407(8)**, 1223-1226.

[44] M Fu, Y Li, S wu, P Lu, J Liu and F Dong. Sol-gel preparation and enhanced photocatalytic performance of Cu-doped ZnO nanoparticles. *Applied Surface Science* 2011; **258(4)**, 1587-1591.

[45] PC Okoye, SO Azi, TF Qahtan, TO Owolabi and TA Saleh. Synthesis, properties, and applications of doped and undoped CuO and Cu_2O nanomaterials. *Materials Today Chemistry* 2023; **30**, 101513.

[46] M Tariq, AK Qureshi, S Karim, M Sirajuddin, N Abbas, M Imran and JH Shirazi. Synthesis, characterization and fuel parameters analysis of linseed oil biodiesel using cadmium oxide nanoparticles. *Energy* 2021; **222**, 120014.

[47] AM Doyle, ZT Alismaeel, TM Albayati and AS Abbas. High purity FAU-type zeolite catalysts from shale rock for biodiesel production. *Fuel* 2017; **199**, 394-402.

[48] SL Abram, I Tavernaro, LJ Johnston, S Zou and U Resch-Genger. Nanoscale reference and test materials for the validation of characterization methods for engineered nanomaterials - current state, limitations, and needs. *Analytical and Bioanalytical Chemistry* 2025; **417(12)**, 2405-2425.

[49] J Hua, M Ji, P Jiao, Z Yin, Q Xia, L Jiang, J Zhang and H Pan. Heterogeneous acid catalysts for biodiesel production: Effect of physicochemical properties on their activity and reusability. *Catalysts* 2025; **15(4)**, 396.

[50] Y Wang, X Wang and M Antonietti. Polymeric graphitic carbon nitride as a heterogeneous organocatalyst: From photochemistry to multipurpose catalysis to sustainable chemistry. *Angewandte Chemie International Edition* 2012; **51(1)**, 68-89.

[51] YMY Al-Ani and M Ahmadlouydarab. Enhancing biodiesel production and tribocorrosion resistance with MWCNT-COOH @TiO_2 nanocatalysts. *Fuel* 2025; **382**, 133811.

[52] T Tamoradi, AR Kiasat, H Veisi, V Nobakht and B Karmakar. RSM process optimization of biodiesel production from rapeseed oil and waste

corn oil in the presence of green and novel catalyst. *Scientific Reports* 2022; **12(1)**, 19652.

[53] MK Lam, KT Lee and AR Mohamed. Homogeneous, heterogeneous and enzymatic catalysis for transesterification of high free fatty acid oil (waste cooking oil) to biodiesel: A review. *Biotechnology Advances* 2010; **28(4)**, 500-518.

[54] MG Jang, DK Kim, SC Park, JS Lee and SW Kim. Biodiesel production from crude canola oil by 2-step enzymatic processes. *Renewable Energy* 2012; **42**, 99-104.

[55] B Gurunathan and A Ravi. Process optimization and kinetics of biodiesel production from neem oil using copper doped zinc oxide heterogeneous nanocatalyst. *Bioresource Technology* 2015; **190**; 424-428.

[56] MA Hazrat, MG Rasul, MMK Khan, N Ashwath, AS Silitonga, IMR Fattah and TMI Mahlia. Kinetic modelling of esterification and transesterification processes for biodiesel production utilising waste-based resource. *Catalysts* 2022; **12(11)**, 1472.

[57] MA Hazrat, MG Rasul, MMK Khan, N Ashwath, IMR Fattah, HC Ong and TMI Mahlia. Biodiesel production from transesterification of Australian *Brassica napus L*. oil: Optimisation and reaction kinetic model development. *Environment, Development and Sustainability* 2023; **25(11)**, 12247-12272.

[58] MR Abukhadra and MA Sayed. K+ trapped kaolinite (Kaol/K+) as low cost and eco-friendly basic heterogeneous catalyst in the transesterification of commercial waste cooking oil into biodiesel. *Energy Conversion and Management* 2018; **177**, 468-476.

[59] VB Veljković, OS Stamenković, ZB Todorović, ML Lazić and DU Skala. Kinetics of sunflower oil methanolysis catalyzed by calcium oxide. *Fuel* 2009; **88(9)**, 1554-1562.

[60] A Pugazhendhi, A Alagumalai, T Mathimani and AE Atabani. Optimization, kinetic and thermodynamic studies on sustainable biodiesel production from waste cooking oil: An Indian perspective. *Fuel* 2020; **273**, 117725.

[61] SG Musharraf, MA Ahmed, N Zehra, N Kabir, MI Choudhary and A Rahman. Biodiesel production from microalgal isolates of southern Pakistan and quantification of FAMEs by GC-MS/MS analysis. *Chemistry Central Journal* 2012; **6(1)**, 149.

[62] V Mittal, KN Talapatra and UK Ghosh. A comprehensive review on biodiesel production from microalgae through nanocatalytic transesterification process: Lifecycle assessment and methodologies. *International Nano Letters* 2022; **12(4)**, 351-378.